Article

Alkali Monitoring of Industrial Process Gas by Surface Ionization—Calibration, Assessment, and Comparison to *In Situ* Laser Diagnostics

Dan Gall,* Jan Viljanen, Ivan Gogolev, Thomas Allgurén, and Klas Andersson

Read Online

ACCESS | Metrics & More | Article Recommendations

ABSTRACT: In this work, we present rigorous calibration and assessment of a surface ionization detector (SID) for alkali monitoring in industrial process gases and compare it to an *in situ* laser diagnostic method called collinear photofragmentation and atomic absorption spectroscopy (CPFAAS). The side-by-side comparison of the time-resolved alkali concentration was performed in a technical-scale gas burner seeded with selected alkali salts, corresponding to alkali molar fractions of 10−100 ppm in the flue gas. The SID operates at room temperature and relies on extraction, dilution, and conditioning of the sample gas, whereas CPFAAS provides *in situ* molecular data. During KCl addition, the instruments were in good agreement: 80.1 ppm (SID) and 88.5 ppm (CPFAAS). In addition to the field measurements, internal validation of SID performance parameters (flow, electric field strength, and filament temperature) and external parameters (particle size and salt composition) was performed. The difference in sensitivity toward different alkali salts was found to be considerable, which limits the quantitative assessment for a sample gas of unknown composition. The results demonstrate the capability and limitations of the SID and show that a SID can satisfactory monitor KCl levels in a process gas over several days of continuous measurements. However, for heterogeneous fuels with deficient characterization of the gas composition, the obtained SID signal is difficult to interpret without supportive diagnostics. The generic ability of the SID to detect Na and K in both gas and particle phases makes it a valuable complement to alkali diagnostics, such as spectroscopic techniques.
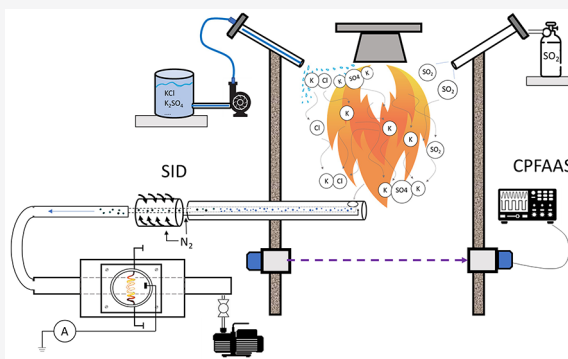
1. INTRODUCTION

The alkali metals sodium and potassium are among the most abundant elements on Earth and known to play an important role in thermal processing techniques as a result of their volatility and reactive nature. Understanding the alkali chemistry and key factors that influence their behavior has been desired by researchers for several decades, and the research has intensified recently as a result of increased interest in biogenic fuels.[1] The partitioning and distribution of alkali compounds in thermal processes varies widely with fuel composition, reactor design, temperature profile, and other process parameters. Of these, the fuel chemical composition is a key factor that influences the fate of alkali, where silicate, Cl, and S are among the most important elements.

Consequently, processing alkali-rich fuels is often considered problematic as a result of the release and subsequent condensation of reactive alkali compounds that cause corrosive damage on industrial equipment. Heat exchangers, catalytic surfaces, and filters exposed to alkali compounds easily become deteriorated by alkali depositions. Alkali compounds may also interfere with the combustion chemistry and can either promote or inhibit the fuel oxidation depending upon specific conditions. For example, the presence of volatile alkali compounds may affect the formation of flue gas pollutants, such as NO_x, SO_2, and CO, by either direct reactions or indirectly by influencing the radical pool.[2−5] In contrast, alkali compounds may also have beneficial effects on the thermal conversion of carbon fuels by increasing the conversion kinetics and reducing the level of unconverted hydrocarbons.[6,7] For example, various additions of alkali metals have been used to increase commercial gasification processes for both coal and biomass.[8] However, the mechanisms and reaction chains are not yet fully determined. Furthermore, available kinetic models rely on several assumptions with the lack of direct measurements for some of the alkali reaction steps.

The alkali-related research has, to some extent, been limited by the lack of adequate alkali diagnostics. The harsh environment and opaque gas streams have limited the ability to apply sensitive equipment and perform detailed investigations, in particular, at large-scale facilities. However, in recent years, a number of novel alkali measurement techniques have evolved,[9,10] and the availability and simplicity of established techniques have increased. This has led to a major increase in detailed alkali research, and numerous studies are to be found in the literature. One of the non-commercial measurement methods found in the literature is surface ionization (SI).

SI is commonly used to create a highly efficient, well-characterized ion source[11] for mass spectrometry applications.[12] The principle was applied by the University of Gothenburg to develop a surface ionization detector (SID) for quantitative alkali measurements used for atmospheric and fuel processing research.[13−16] The simplicity, high selectivity toward alkali atoms, and wide measurement range are the main advantages with SI techniques. The simple and low-cost SID has been developed and applied by other research groups for combustion and gasification research.[17−19] Several SI studies are available in the literature, and the applicability of the methodology for alkali-containing aerosols has been proven. Most of the reported work has been made by the University of Gothenburg[15,20] and includes the development, optimization, and calibration, which are the initial steps in the development cycle of a new analytical technique. The key feature of SI-based analytics is the metal filament, where alkali compounds melt, dissociate, and desorb. The physical properties of Pt (low oxidation potential and low work function) make it an ideal candidate for continuous alkali monitoring, although several different filament materials and geometries have been explored. A few different cell designs have been described.[13,17,18,21−23] The most common application uses a Pt spiral encapsulated in metal housing at room temperature and atmospheric pressure, where the sample gas is directed. To control the flow pattern and increase the amount of alkali particles that interact with the filament, different cell designs have been evaluated. Davidsson et al.[13] use a Pt wire mounted in the measurement cell, in which the sample gas is expanded to increase the turbulence and, thereby, the interaction between the alkali particles and the Pt metal. Gogolev et al.[19] use a Pt wire across a laminar sample flow to reduce the influence of various flow patterns to increase stability and robustness. Wellinger et al.[17] use a grid of Pt wire to obtain a uniform alkali−Pt interaction. Other applications use a heated measurement system to avoid challenges associated with extraction and dilution. Recently, Ji et al.[18] used a Pt filament inserted in the gas flow, as a probe, to continuously measure Na and K. Furthermore, a SI technique has been developed to enable discrete measurements of Na and K, by rapidly reversing the electric field.[10] The feature may be added independent of the design, however, with increased complexity and reduced time resolution (0.1 Hz compared to >1 Hz). The quantification of a SI ion signal has been performed with side-by-side measurement of pure alkali salt aerosols, using commercial aerosol diagnostics to obtain the mass concentration per volume. This calibration procedure has inherent uncertainty factors associated with the aerosol generation and the particle morphology and density. Therefore, it is of interest to perform comparative field measurements using a SI-based instrument alongside an independent alkali analytical technique, such as optical spectroscopy.

Laser diagnostics enable online *in situ* monitoring of alkali species in high-temperature process gases, as extensively reviewed by Monkhouse.[24] Photofragmentation and laser-induced fluorescence (PF−LIF) has been applied in alkali species monitoring and imaging in laboratory-scale burners and small-scale combustion units.[25,26] However, its application to industrial-scale units has been challenging. In contrast, tunable diode laser absorption spectroscopy (TDLAS) has been widely applied in different scale reactors for alkali monitoring.[27,28] TDLAS detection capability is limited to atomic alkali species that restrict alkali analysis in general in process gases. Molecular alkali species have been monitored using differential optical ultraviolet absorption (UV-DOAS)[29] and collinear photofragmentation and atomic absorption spectroscopy (CPFAAS).[30] As a result of the overlapping spectra of alkali chlorides NaCl and KCl and hydroxides NaOH and KOH, respectively, UV-DOAS provides information mainly on the total alkali species content. CPFAAS is capable of distinguishing between potassium and sodium species. Recently, a photofragmentation method was combined with the TDLAS method, enabling simultaneous monitoring of atomic and molecular potassium species in high-temperature process gases.[31]

While some of the optical methods are calibration-free, other methods require internal calibration using reference samples. In this process, the performance characteristics, commonly, working range, selectivity, trueness, precision, and limit of detection, are examined and optimized. Because no alkali measurement standard is commercially available, each laboratory must produce its own, which generates ambiguities and difficulties to compare studies within the field. To increase the level of confidence for a given analytical technique, comparative measurements with a separate analytical technique, often referred to as collaborative studies, are preferred.[32] However, a direct comparison of different alkali analytical techniques may be difficult, owing to the significant differences between the available measurement principles. Consequently, external validation studies of alkali analytical techniques are scarce. Monkhouse et al.[21] performed simultaneous alkali flue gas monitoring with SI and photofragmentation fluorescence; however, the investigation focused on alkali phase discrimination in the parts per billion (ppb) range, using the systems as complements rather than a strict comparison. Moreover, comparing extractive methods to non-intrusive *in situ* measurements may shed light on the difficulties with extraction and conditioning a gas sample containing either alkali vapors, alkali aerosols, or their mixture. Most extractive methods require significant dilution and cooling and, therefore, suffer from artifacts that may be difficult to correct.[33,34]

In this study, emphasis is put on SID calibration and differences in signal sensitivity to different alkali molecules to assess the analytical abilities of SID to operate on industrial process gases containing various alkali species. Furthermore, an alkali-seeded technical-scale gas flame was simultaneously characterized by two independent alkali-monitoring systems: SID and CPFAAS. SID detects a signal proportional to the molar concentration (ppm) of alkali in the extracted sample gas, while the CPFAAS captures *in situ* the molar fraction of KCl and KOH molecules in the gas phase. This arrangement enables the evaluation of the SID extraction system and evaluates if a stand-alone SID can provide reliable alkali diagnostics under varying process conditions.
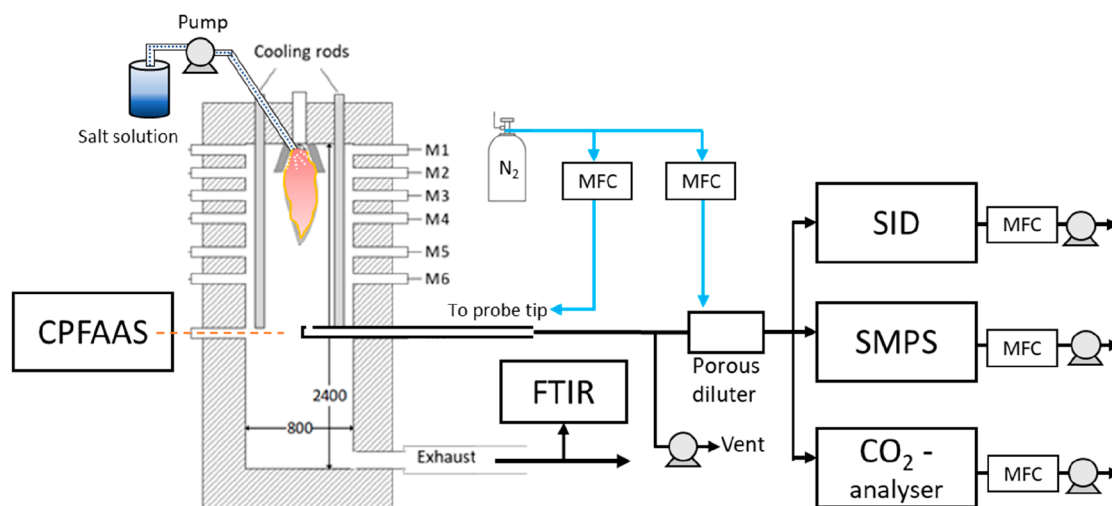
Figure 1. Schematic illustration of the Chalmers 100 kW combustion facility with deployed diagnostics. The laser beam and SID probe are inserted perpendicular to each other.

2. EXPERIMENTAL SECTION

2.1. Facility and Instrumentation. The tests were performed in the Chalmers 100 kW combustion unit, described in detail elsewhere.[35,36] The reactor is cylindrical with a diameter of 0.8 m, and measurement ports are located at seven different distances along the vertical flame axis on four sides of the unit. The temperature profile is measured with suction pyrometry with a maximum of 1750 °C in port 2 and thereafter decreasing to 750 °C in port 7. Propane was used as fuel, with λ of 1.15 and with a resulting flue gas composition composed of 11.8 vol % CO_2 (dry), 2.95 vol % O_2 (dry), and 14.6/13.6 vol % H_2O, for operation with and without liquid injection, respectively. The used operating conditions are consistent with established conditions used in previous work, in which a detailed temperature profile and gas composition are available.[5] Alkali salts are injected as a liquid, and the flow rate is set and monitored using a pump (delta 1612, ProMinent). To achieve a stable reference concentration, 0.9 L h^{-1} KCl(aq) with a concentration of 3.34 wt % was injected, which corresponds to 100 ppm of KCl in the flue gas, assuming complete combustion and that all injected KCl remains as KCl. The concentration was varied by adjusting the concentration of the injected liquid while keeping other parameters constant. For KCl, the concentration is controlled over time by a hand-held digital refractometer (PAL-49S, Atago) to ensure constant conditions. Similar experiments have been performed in previous research, and the conditions are well-defined. A schematic of the combustion system and the measurement points are given in Figure 1.

The SI technique has been demonstrated in previous studies and applied in industrial applications, such as combustion, gasification, and chemical looping processes.[13,17,22,23,37] A detailed description of the methodology can be found elsewhere.[20] In brief, the sample gas flows through a chamber with a hot metal surface, where a fraction of the aerosol particles impinges, decomposes, and desorbs as a result of the high temperature (typically ~1500 K). The selectivity toward alkali atoms is very high as a result of their low ionization potential.[38] Thus, the corresponding ion signal is proportional to the amount of alkali atoms present in the sample gas. The SID used in this study has previously been used in chemical looping research.[23]

To obtain a mass concentration (mg/m^3) of alkali, the observed ion signal is calibrated using the aerosol mass concentration measured by a scanning mobility particle sizer (SMPS) system (TSI 3082) consisting of a differential mobility analyzer (TSI 3081) and a condensation particle counter (TSI 3750) using a soft neutralizer (TSI 3088). The test aerosol was generated with a constant output atomizer (TSI 3076), and the gas stream was diluted with nitrogen gas before being split and directed to the two instruments. A similar setup has been used in previous investigations,[10,22] and both the

SMPS and atomizer are well-characterized commercial units. However, to convert the measured number concentration to a mass concentration, both the particle shape and density are required. Consequently, these factors are key uncertainties during the calibration procedure. The synthesized aerosol is generated from separate aqueous solutions containing the following alkali salts (used as received): KCl, K_2SO_4, KNO_3, and KOH. The solution is atomized in such a way that large particles are removed by impaction, whereas smaller droplets escape via the gas stream and pass through a diffusion drier where the liquid is removed. The remaining salt residue crystallizes and constitutes the aerosol particles used for calibration. The stability of the generated aerosol was verified by two independent SMPS systems used in parallel.

In addition to the field measurements, some of the inherent SID parameters (temperature, flow rate, and electric field strength) were individually assessed in a controlled environment. The filament temperature has a significant influence on the generated ion signal, and its surface temperature is measured by an optical pyrometer (Optris CT). During the field measurements, the temperature is manually controlled by ohmic heating using a 5−6 A current. The operating temperature was set to 1150 °C to increase longevity of the wire. The sample flow rate through the SID unit is 0.5 liter per minute (lpm) and controlled by a mass flow controller (MFC, Bronkhorst, 0−5 lpm range). A positive voltage between the filament and detector plate is generated by a separate voltage supply. The strength of the generated electric field is controlled by altering the electric potential. The instrument settings used for the SID during the comparative measurements are given in Table 1.

Table 1. SID Settings Used during the Measurements

parameter	value
filament temperature (°C)	1150
sample flow rate (lpm)	0.5
bias voltage (V)	+300
data collection rate (Hz)	1

In addition to the SID, flue gas KCl and KOH concentrations were monitored using a laser-based *in situ* alkali measurement method called CPFAAS.[30,39] The laser light line of sight passed the center of the combustor (10 cm away from the SID sampling point), providing the average KCl and KOH concentrations over the measurement line of sight of port 7. Similar measurement arrangements were previously demonstrated by Viljanen et al. in a coal-fired pilot-scale combustor.[40] The atomic potassium probe laser emitting at the potassium D2 line at 766.5 nm is wavelength-modulated with a 10 Hz sawtooth pattern

to sweep across the line to enable tuning of the measurement sensitivity. The modulation wavelength was monitored by recording the temporal transmission of the probe beam wavelength through a reference potassium cell (SC-K-19375-Q-W, Photonics Technologies). The pulsed fragmentation lasers emitting at 266 nm (FQSS-266-200, CryLas GmbH) and 355 nm (Ultra Big Sky series, Quantel) were timed with the probe laser wavelength sweep, so that the probe beam absorption cross section corresponded to $\sigma_{K,266} = 3.51 \times 10^{-17}$ m^2 and $\sigma_{K,355} = 6.62 \times 10^{-17}$ m^2, respectively. The potassium D2 line shape in the flue gas conditions was determined by injecting 100 ppm of KNO$_3$ to the flame that resulted in a free atomic population to the level of port 7 that could be detected in the temporal probe beam transmission signal. Because the particle load is low during these measurements and the laser unit and detector unit distance was only around 2 m, the laser beam sizes could be adjusted to be small in diameter without compromising the beam transmission through the unit or facing problems with beam divergence. Thus, the pulsed laser beams at 266 and 355 nm had diameters of 11.5 and 5.5 mm, respectively. The temperature at the measurement level is approximately 800 °C. Therefore, the KCl and KOH absorption cross sections for fragmenting laser pulses used in this work are $\sigma_{KCl,266} = 0.74 \times 10^{-21}$ m^2,[41] $\sigma_{KOH,355} = 0.15 \times 10^{-21}$ m^2,[39,42] and $\sigma_{KOH,266} = 0.1 \times 10^{-21}$ m^2.[39,42,43] The precursor molecule concentration X_{prec} is computed using eq 1 that takes the extinction of the fragmenting beams into account[44]

$$X_{prec} = \alpha L_{max} \frac{A_f}{E_{in} L} \frac{hc}{\gamma \lambda_f} \frac{kT}{p} \frac{1}{\sigma_K \sigma_{prec}} \frac{\ln\left(\frac{E_{in}}{E_{out}}\right)}{1 - \frac{E_{out}}{E_{in}}} \quad (1)$$

where αL_{max}, A_f, E_{in}, L, h, c, γ, λ_f, k, T, p, σ_K, σ_{prec}, and E_{out} are the maximum increase in the probe beam absorptivity after the fragmenting laser pulse, the area of the fragmenting beam, the energy of the fragmentation laser pulse at the furnace input, the interaction length of the beams and the sample, i.e. the furnace diameter, in this case, Planck's constant, the speed of light, the photofragmentation efficiency, the fragmentation wavelength, Boltzmann's constant, the sample temperature, the sample pressure, the absorption cross section of potassium, the absorption cross section of the corresponding precursor molecule, and the energy of the fragmentation laser pulse at the furnace output, respectively. The photofragmentation efficiency is assumed to be unity for both KCl and KOH.

2.2. Extraction, Conditioning, and Dilution. A temperature-controlled probe was used for extracting sample gas from port 7. The probe has several small openings around the inlet to dilute and quench the sample gas immediately as it flows into the probe. The sample gas was diluted and rapidly cooled immediately at the probe tip inlet with an overflow of dilution gas, i.e., a higher flow of nitrogen gas compared to the suction, to achieve a rapid aerodynamic quenching. The idea is to create a "sea" of cold inert dilution gas that quenches and dilutes the sample as well as covers the inner walls of the probe. Part of the hot process gas will blend with the nitrogen gas and be transported/embedded by the dilution gas toward the instruments. A simplified illustration of the flow in the probe tip is given in Figure 2. The extraction principle has been used in previous research, and Jiminez et al.[33] found the aerodynamic quenching method to be favorable for extraction of condensable vapors in comparison to other techniques. The probe has been used in previous aerosol research.[37,45] The probe temperature was controlled to 150 °C by an external heater/cooler during the measurement. To examine the amount of deposition losses, the probe was rinsed with purified water before and after each day. The probe rinse was diluted 20 times and analyzed with inductively coupled plasma mass spectrometry (ICP−MS, Thermo iCAP Q), and signal intensities for elemental mass were analyzed with ICP−MS (Thermo iCAP Q) and inductively coupled plasma optical emission spectrometry (ICP−OES, Thermo iCAP 6500) for elements in the ppb and parts per million (ppm) ranges, respectively. For both methods, three readings of signal intensities were made to give an average value with standard deviation. Standards were prepared from either 10 or 1000 ppm
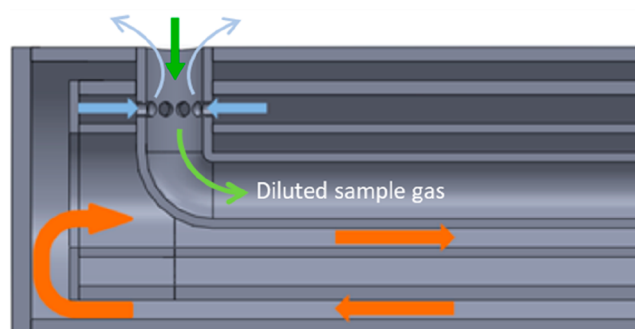

Figure 2. Cross-sectional drawing showing the tip of the particle-sampling probe used in this work. The green arrow indicates the sample flow through the probe inlet. The blue arrows represent the inert dilution gas (N$_2$), and the orange arrows indicate the flow of thermal oil to control the probe temperature. This figure was reproduced with permission from ref 37. Copyright 2017 Elsevier.

certified elemental standards (Ultra Scientific, VHG Laboratories, and CPA Chem). The standard series were prepared in two versions: one with a blank solution diluted 20 times for use with the samples and one without any blank addition. The blank background concentrations were evaluated from the difference in calibration curve intercepts for the two series, and detection levels as 1σ error of the intercepts.

Downstream of the probe, a porous cylinder diluter was used to further dilute the sample gas with nitrogen gas before it was split to the different instruments. At this point, alkali vapors have transformed to aerosol particles by either homogeneous nucleation or condensation and subsequent agglomeration.[46] The porous diluter reduces wall depositions and allows for adjustable flow rates, which can be used to fine tune the total dilution ratio.[47] Both dilution flow rates were controlled by MFCs (Bronkhorst EL-Flow Prestige).

To determine the dilution ratio, CO$_2$ levels of the diluted sample was measured (LI-COR LI-850) and compared to the CO$_2$ measurements of the undiluted gas. The undiluted CO$_2$ concentration was measured with a Fourier transform infrared spectroscopy (MKS MGS3000) extracted downstream of port 7. The CO$_2$ concentration was also measured in port 7 to ensure even distribution and a representative concentration in the downstream port. The accuracy of the CO$_2$ analyzers is <1.5 and <0.5% of the reading for LI-COR and FTIR, respectively. The uncertainty in the CO$_2$ measurement will directly contribute to the total SID measurement error during field measurements.

3. RESULTS AND DISCUSSION

3.1. Calibration and Assessment of SID Properties. The variability of key inherent parameters used in the analytical procedure was assessed to understand how they influence the ion signal. The filament temperature, sample flow rate, and electric field strength were individually varied, while other parameters were kept constant. The relative error of each parameter was combined, assuming independence, and used to represent the random error, e.g., the precision of the instrument. Throughout the calibration, the synthesized aerosol was monitored with two SMPS systems to ensure the stability of the aerosol generation.

To investigate the effect of the Pt surface temperature, the heating current amperage was varied to generate a surface temperature of 700−1200 °C. Figure 3 shows the obtained ion signal (nA) per potassium mass concentration (μg m^{-3}). For KCl and KNO$_3$, a steady signal increase is observed from around 800 to 1125 °C. Thereafter, the signal decreases until around 1160 °C, where it again shows a positive correlation with the Pt temperature. The reason for the signal reduction at
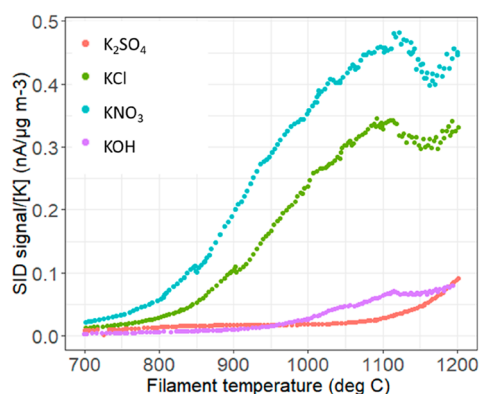
Figure 3. Influence of the filament temperature on the ion signal per mass concentration of potassium, for selected alkali salts.

1125 °C could not be attributed to any single SID instrument parameter or properties of the salts used. Because this signal reduction is consistent and repeatable, it does not impede the measurement function of the instrument and was accepted as an inherent attribute of the instrument. For K_2SO_4, only a minor signal is detected up to around 1050 °C. Above 1050 °C, a steady increase of the ion signal is observed. It is known from previous investigations that the higher thermal stability of alkali sulfates limits the ionization at lower temperatures, resulting in lower signal intensities per alkali mass concentration.[10] The low KOH signal is somewhat surprising and is discussed in further detail below. Note that the amplitude of the signal intensities (nA/[K]) is quantified on the basis of the shape and density assumptions required to quantify the aerosol mass concentration, discussed in further detail below. Nevertheless, it does not influence the shape of the obtained ion signals.

The results suggest that the surface temperature may be used to separate some of the species by simply adjusting the filament temperature. The selection of a suitable filament temperature depends upon the application and sample composition. Aging effects of the Pt filament should also be considered, where a higher surface temperature reduces the lifetime of the filament by increasing the oxidation rate. During field measurements, the observed filament temperature varies with discrepancies in the heating current and sample gas flow rate. Throughout the field measurements, the mean temperature was 1157 ± 4.7 °C, which corresponds to a variation in the ion signal of ±0.9% for KCl.

The effect of sample flow was investigated by changing the MFC flow rate and manually adjusting the heating current amperage to keep a constant filament temperature. The result of the flow rate investigation is presented in Figure 4. As seen in the figure, a linear relation with a slope coefficient of 1.02 and intercept of 0.07 was found between the ion signal/[K] and flow rate (lpm), as expected given the increased amount of analyte passing through the measurement cell. The significant non-zero intercept indicates a deviation from linearity at flow rates of <0.3 lpm, which is also seen by the deviation from the nominal value. During operation, a flow rate of 0.5 lpm was used, to increase the longevity of the filament. Increasing the flow rate generates a higher ion signal; however, it requires a higher heating current amperage and may therefore reduce the lifetime of the filament. The accuracy of the mass flow rate is ±1.5% (provided by the manufacturer), which represents a measurement error of ±1.5% based on the established linear
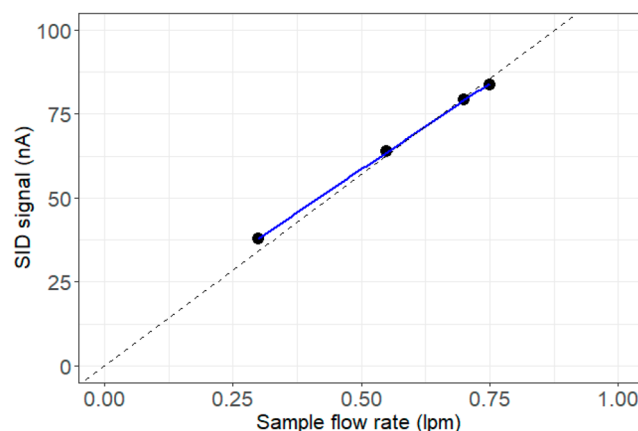

Figure 4. Effect of the sample flow rate using a constant KCl test aerosol. The Pt surface temperature was kept constant (1150 °C) by adjusting the heating current through the filament. A linear relation (solid line) was obtained by least squares regression illustrated together with the theoretical relation (dashed line).

relation. However, variations in the flow rate would also propagate to the filament surface temperature as a result of the change in heat transport. The extent of the uncertainty factor interaction was not investigated further.

To investigate the effect of the electric field potential, the bias voltage was altered between +150 and +500 V, and the result is given in Figure 5. The bias voltage creates the electric
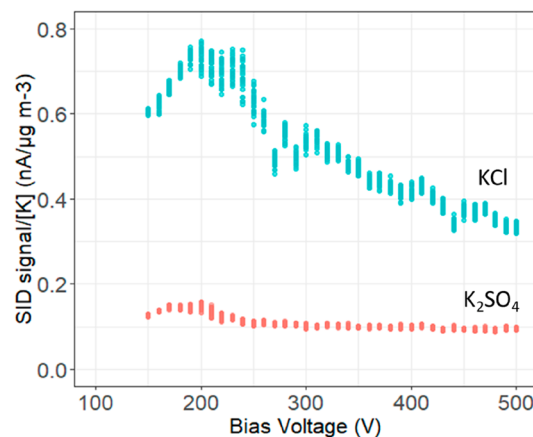

Figure 5. SID ion signal per mass flow of K as a function of bias voltage using a steady flow of KCl and K_2SO_4 aerosols. The signal intensity reaches a maximum at around +200 V.

field in which the generated ions are repelled from the filament surface, where a fraction impacts the collector plate. The maximum ion signal for both investigated salts was around +200 V, where 9.0 and 1.7% of the potassium atoms entering the SID reach the collector plate for KCl and K_2SO_4, respectively. The reason behind this relation is not clear, and the electric field and ion flow pattern have not been investigated further. During field measurements, the electric potential was controlled to +300 V by an external voltage supply and monitored with a multimeter. The variation in electric potential was ±1.7%, which corresponds to an ion signal variation of ±0.8% for KCl.

Combining the relative errors from each parameter gives an estimated precision (for pure KCl aerosols) according to

$$\varepsilon_R = \sqrt{(\varepsilon_{Temp}^2 + \varepsilon_{Flow}^2 + \varepsilon_{Bias}^2)} = 1.9\%$$

This can be compared to the standard deviation of 2.47%, obtained from continuous SID sampling on a steady KCl aerosol flow of 85 μg m^{-3} during 600 s.

Besides the internal parameters, two external factors were investigated: selectivity toward different alkali salts and influence of the aerosol particle diameter. It is known that SI-based techniques have a high selectivity toward alkali metals. On the basis of the Langmuir−Saha equation,[48] the degree of ionization of alkali metals compared to non-alkali metals present in the sample gas (i.e., alkali earth metals, organics, etc.) is several orders of magnitude higher. However, to investigate the sensitivity for different alkali salts, a test aerosol for each compound was generated individually and the ion signal was correlated to the mass concentration measured by the SMPS. Each measurement point was averaged over 120 s and repeated 3 times. The result is presented in Figure 6.
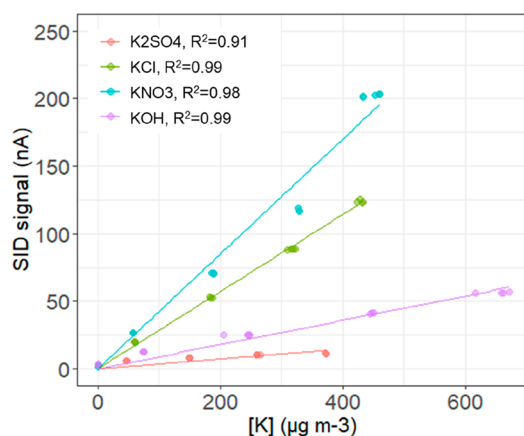

Figure 6. SID sensitivity for selected alkali salts. Test aerosols were generated by liquid spray and diffusion drying, and the aerosol mass concentration is measured using a SMPS system. The linear fits were obtained by least squares regression.

The potassium mass concentration given by the SMPS was determined using bulk density and assuming spherical particles. Of the investigated salts, KNO$_3$ and KCl induced the highest ion signal per mass concentration of potassium. The relatively lower sensitivity for KOH was unexpected. One possible explanation for this behavior is that synthesizing KOH particles in air may cause reactions with ambient CO$_2$, producing fractions of K$_2$CO$_3$ and KHCO$_3$, as observed in previous research.[49] When the KOH−K$_2$CO$_3$−KHCO$_3$ droplets are dried, a degree of crystal H$_2$O may be present. The bound water would be perceived as K mass by the reference measurements (SMPS). Overestimation of the true K mass would result in underestimation of the SID response to KOH aerosol. Sensitivity toward K$_2$SO$_4$ was the lowest of the tested aerosols. We believe that the lower sensitivity is associated with the high thermal stability and, thus, higher resistance for the aerosol particle to melt and dissociate. Of the individual least squares regression lines, KCl and KOH showed the highest degree of linearity ($R^2 > 0.99$). However, without knowledge of alkali speciation, the non-linearity as a result of the difference in sensitivity makes quantification impractical.

Finally, the influence of the aerosol particle diameter was investigated in two independent experiments: first by size

selection using a tandem differential mobility analyzer (DMA) setup and second by shifting the entire size distribution by increasing the KCl concentration in the atomized liquid. During the tandem DMA test, the scanning SMPS system was operating on a 10:1 (sheath/sample) flow ratio to optimize the transfer function, which limits the measurement range regrading the particle diameter. Within the observed particle diameter size range, no apparent influence was observed, although some variation is visible, as seen in Figure 7.
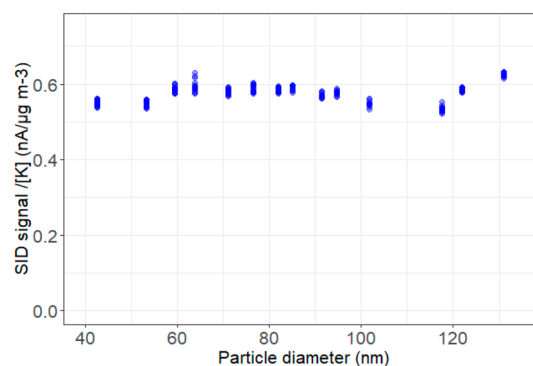

Figure 7. Influence of the aerosol diameter on the SID signal investigated with size-selected KCl aerosols by tandem DMA. Within the valid observation range, no significant influence by the particle size is apparent.

However, the monodispersity of the test aerosol using a tandem DMA approach is dependent upon the primary distribution, and influence of the secondary peak (i.e., double-charged particles) may be significant. A different method to generate a true monodisperse aerosol, e.g., with an additional DMA, over an increased size range would be beneficial to study the size effect in further detail.[50] The second test, shown in Figure 8, in which the median mass was increased from 100 to 150 nm clearly showed a size dependency, where the test aerosol with a median mass at 100 nm resulted in a higher signal response compared to the median mass at 150 nm. Previous investigations on the influence of the particle diameter are not cohesive,[10,15,51] suggesting that the relation is dependent upon the specific SID design and flow trajectory.

In summary, the internal assessment displayed an acceptable variation in signal intensity for the filament surface temperature, sample flow rate, and bias voltage. Assessment of external parameters showed that quantification of an unknown alkali species is not possible with the current design as a result of large variations in selectivity toward different alkali salts. In addition, supportive measurement of the aerosol size may be required, because size dependency was observed for particles within the size of freshly nucleated aerosols, typically formed during extraction and cooling of high-temperature alkali vapor.

3.2. Field Results. 3.2.1. Time Series. Process gas was continuously extracted during 6 h for 2 consecutive days, and the time series with 1 Hz resolution during day 1 is illustrated in Figure 9. The SID ion signal (nA) is converted to molar fraction (ppm) using the calibration curve for pure KCl aerosols, described below, and multiplied with the dilution factor. Because no correction was applied for selectivity with respect to different alkali salts, the result is presented as KCl equivalents, i.e., the corresponding mass concentration per volume for KCl aerosols in the valid aerosol particle diameter
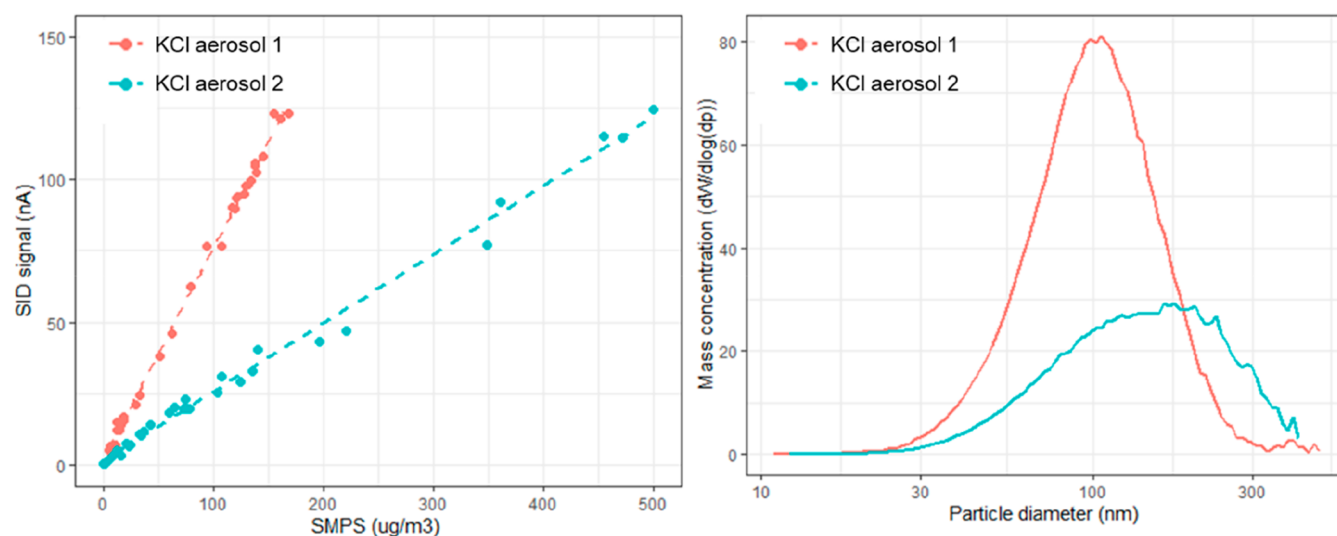
Figure 8. Size dependency was investigated using synthesized KCl test aerosols with different size distributions. (Left) Calibration line for the two different size distributions showing the higher sensitivity for the mass size distribution with a higher median mass diameter (e.g., larger particles). (Right) Aerosol mass size distribution of the two KCl aerosols.
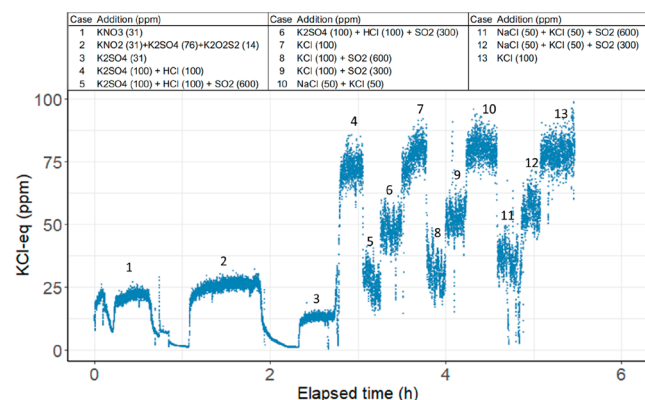

Figure 9. Time-resolved SID data (1 Hz) during different additions of selected alkali salts. During the addition of alkali chlorides, the SID signal corresponds well with the nominal concentration. The lower signal response of sulfates demonstrates the quantification limitation when sampling an unknown gas composition.

range. Additions of potassium nitrates, sulfates, and chlorides were injected to the top of the flame, and the time periods for the various additions (cases) are indicated in the figure. During chloride additions, two levels of SO_2 (300 and 600 ppm) were added simultaneously to observe sulfation effects of the alkali halides and their influence on the ion signal.

As seen in Figure 9, the additions of different alkali salts are captured by the fast response time of the SID. The rise and fall time of the SID instrument is adequate to observe the transient process in seconds. The lower fall time seen in, e.g., the end of cases 1 and 2 is due to diffusion mixing when the alkali solution is substituted to water. The given ppm values for the various additions are calculated using combustion fuel and air flow, assuming complete evaporation of the added salt solution. The fluctuations in case 1 are caused by unsteady flow of the liquid injection, which was otherwise stable over the measurement period. During case 2, combustion settings were changed to oxygen-enriched air combustion, which gave a moderately lower SID signal compared to cases 1 and 3, with respect to the mass of potassium added. In general, additions

of chlorides and nitrates resulted in a reasonable agreement between the added mass of potassium and observed concentrations by the SID as a result of high SID sensitivity and favorable extraction settings (i.e., rapid nucleation at the probe tip). The observed SID signal is drastically lower when a similar amount of potassium is added as sulfate, owing to the lower sensitivity toward sulfates. Furthermore, when a high level of SO_2 is added in combination with KCl, the ion signal declines to similar values as for sulfate additions, indicating a high degree of sulfation. When the SO_2 addition is reduced to 300 ppm, the SID signal partly recovers. We believe that the lower sensitivity for K_2SO_4 compared to KCl is the main reason for the signal decay. The variation in the ion signal shows a key limitation in quantification when sampling an unknown gas composition. In contrast, the instrument feature may be a valuable analytical tool for studying the K–Cl–S chemistry, if the gas composition is characterized by complementary diagnostics.

3.2.2. Comparative Measurements with CPFAAS. During the addition of KCl, the reported mass concentration by the SID can be directly compared to the CPFAAS system. The participating analytical techniques measured the process gas independent of each other, and the obtained values are assessed and compared for the different cases. The observed mean and variance during the addition of three different chlorides during 300 s are given in Figure 10. The SID concentration is continuously measured and logged every second as single points. The CPFAAS data are collected during an injection case in two 50 s long sequences with 10 Hz repetition rate. The data are averaged over 1 s to obtain 100 measurement points to compare to the SID measurement.

During the addition of KCl, the obtained concentrations are in satisfactory agreement: 80.1 ppm (SID) and 88.5 ppm (CPFAAS). However, a direct comparison is convoluted by inherent differences in the analytical techniques that should be taken into account. The CPFAAS system provides information on the absolute concentration of KCl and KOH, while the SID provides information on the total alkali content in the gas. In addition, the analyte is diluted and cooled to 25–30 °C prior to the SID analysis, whereas the CPFAAS analyzes the hot
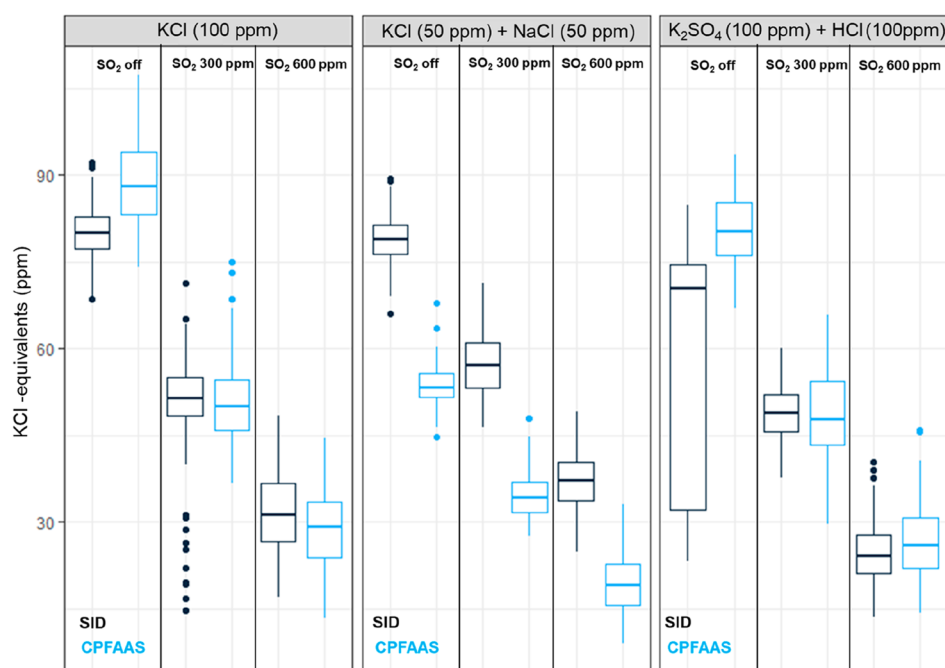
Figure 10. Comparison of values obtained with SID (total alkali) and CPFAAS (KCl) for different additions of alkali salts at different SO_2 loadings with the mean (horizontal line), upper and lower quartiles (lines), and outliers (dots). During the KCl additions, results from the measurement systems are in reasonable agreement.

process gas *in situ*. The extraction and rapid cooling may transform alkali species present at high temperatures, such as K and KOH, given their high reactivity toward CO and CO_2. However, throughout the side-by-side comparison, no KOH was observed by the CPFAAS. Given the satisfactory agreement between the analytical systems, the correction for extraction dilution and conditioning appears to be adequate.

To identify the reactor center position, the probe was carefully inserted until the laser signal was blocked and, thereafter, reversed 5 cm to not interfere with the laser measurements. At this measurement position, the gas is assumed to be well-mixed, and the sample point was used for the comparison measurements. To investigate possible fluctuations across the measurement plane, the probe was traversed across the horizontal axis, while all sampling conditions were kept constant. Close to the reactor wall, a reduction of 19% was observed; otherwise, no detectable decay of the signal was noticed. By traversing the probe, SID measurements can provide the concentration profile across the measurement plane, whereas the CPFAAS technique reports the mean concentration along the plane. Obviously, the option to traverse the probe and observe the concentration profile can be valuable to gather information in non-uniform gas flows.

Besides pure KCl, the addition of internally mixed alkali chloride is also an interesting case regarding measurement evaluation. When a 50:50 mixture (molar basis) of NaCl and KCl is added, the observed CPFAAS concentration is reduced to 53.9 ppm compared to 88.5 ppm for pure KCl addition. In contrast, the SID reports similar concentrations, 80.1 (KCl) and 78.9 ppm (NaCl/KCl), which reflect the instruments inability to discriminate between Na and K. The somewhat lower value when NaCl is present relates to the lower ionization probability for Na (89%) compared to K (99%) on a Pt surface.[52] The feature to measure the total alkali content (Na + K) may be useful and reflects the SID versatility. In

addition, with the application of the field-reversal technique, the SID is able to differentiate between NaCl and KCl as a result of differences in their surface desorption kinetics.[10]

When SO_2 is added, a clear decay in the KCl concentration is apparent for both measurement techniques. The decay in the KCl concentration observed by CPFAAS is a direct indication of the occurring sulfation process in the flue gas. For SID, however, the decay in the alkali signal is mainly due to the lower sensitivity toward sulfates compared to KCl. In addition, the total aerosol mass concentration measured by the SMPS system also reports a decreased mass concentration from the SO_2 additions. It is possible that the presence of SO_2 influences the gas-to-particle transition during the extraction process, which can increase losses by impaction and condensation in the sampling lines. However, from the particle size distributions (discussed below), it does not appear as a significant shift toward larger particle sizes.

3.2.3. Auxiliary Measurements. To support SID data evaluation, the particle size distribution was monitored by the SMPS system with a scan time of 120 s. The obtained number and mass size distributions for the different additions are illustrated in Figure 11 as an average over several consecutive scans. The mass size distribution is estimated from the measured number concentration assuming spherical particles and uniform density. During KCl additions, a bimodal distribution is observed, with a distinct nucleation mode and a following accommodation mode. The nucleation mode declines with reduced levels of KCl and is not observed for KNO_3 addition. The nucleation mode is generated in the probe tip, where the alkali vapors are exposed for a rapid cooling rate by the nitrogen gas, and the influence of alkali speciation was not investigated further. The freshly nucleated particles grow by agglomeration and condensation, which generate the accommodation mode centered around 200 nm. Particles within this mode are less sensitive toward residence
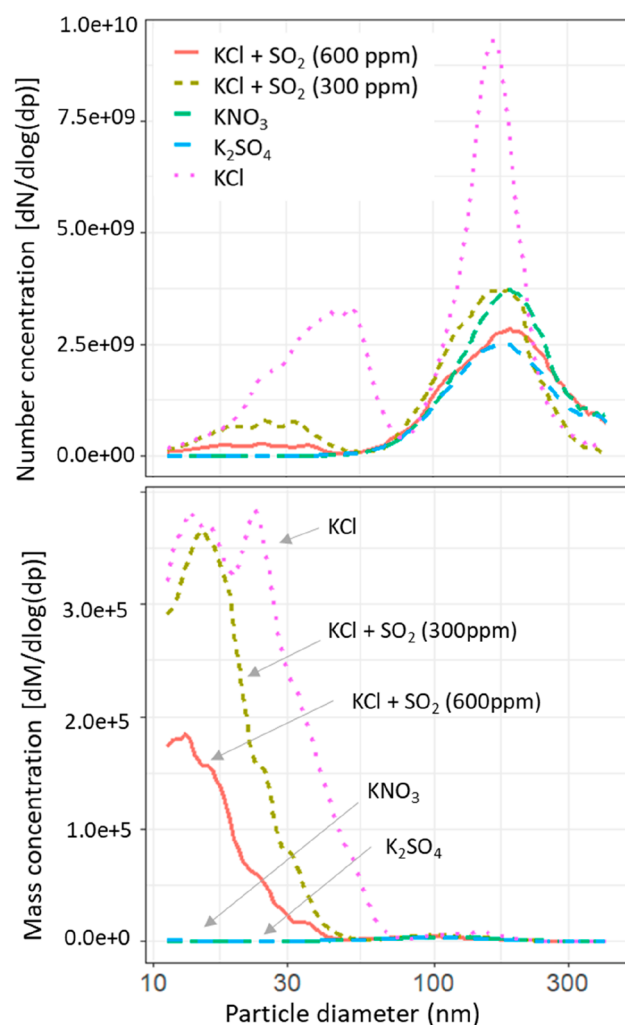
Figure 11. Particle size distributions of the extracted aerosol during different additions. During KCl addition, the extraction generates a bimodal distribution with a dominant mass fraction between particle diameters of 100−300 nm. KCl generates a distinct nucleation mode (d_p of <50 nm), which reflects the prompt nucleation of alkali halides. The nucleation mode diminishes as SO_2 is added and is not observed during K_2SO_4 or KNO_3 addition.
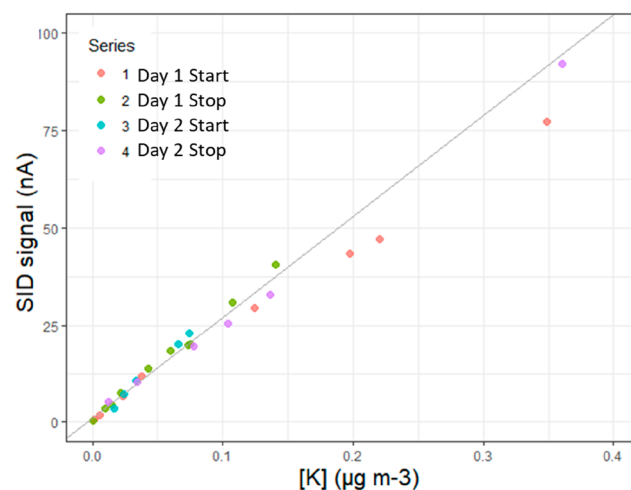

Figure 12. Calibration data for the SID performed at the start and end of each measurement day. The calibration curve is a Deming regression based on all measurement points ($R^2 = 0.99$).

time in the sampling system compared to the nucleation mode (particle diameter of ∼30 nm), which can more easily diffuse toward the sample line wall and become lost by deposition.[53] The aerosol distribution obtained during field measurements, generated by nucleation of alkali vapor, differs from the aerosol distribution used during calibration (Figure 8). Using a similar aerosol size distribution for calibration (i.e., from condensed vapor) would improve the SID accuracy.

3.2.4. Field Calibration of the SID. The SID was calibrated directly at the start and stop of the measurement day using the procedure described above. The calibration data for 2 consecutive days, given in Figure 12, were combined to fit a single Deming regression line ($R^2 = 0.99$) with the following expression:

$$Y = 0.3x \pm \varepsilon$$

were Y is the estimate KCl concentration (mg m^{-3}), x is the obtained SID signal (nA), and ε is the measurement error. At high KCl loadings (>0.1 mg m^{-3}), the SID signal shows a nonlinear tendency as a function of the KCl concentration,

most likely as a result of space charge limitations. During field measurements, the sample gas was diluted with sufficient inert gas to retain the linear relation. The reference measurement (SMPS) requires both shape and density for a quantitative assessment of the aerosol loading. The physical properties of the produced particles depend upon the atomization method, temperature, and properties of the surrounding gas.[54] Because the actual shape and density of the synthesized particles are unknown, we used the dynamic shape factor of a sphere and the salt bulk density. If known, the dynamic shape factor can be used to correct for the difference in drag force between irregular, non-spherical particles and spherical particles. Previous investigations on diffusion dried nanoparticles from a atomized liquid showed that surface properties and porosity are dependent upon the aerosol diameter, and particles with a diameter of <50 nm are the subject of the largest deviation from unity.[55] The particle size distribution of the test aerosol used for calibration is centered around 150 nm, hence, assuming a spherical geometry with bulk density is reasonable. As seen above, the quantified ion signal is in line with the independent optical measurements, which demonstrates the applicability of the calibration procedure for SID KCl measurements.

3.2.5. Correcting for Dilution and Losses in the Extraction System. The sample gas must be extracted from the reactor, diluted, and cooled to ambient temperature before it can be analyzed by the SID. Any modifications on the sample, e.g., dilution, have to be corrected. The precision of the dilution ratio of the extracted sample gas is critical because any measurement error would propagate directly to the concentrations reported by the SID. It is challenging to obtain a representative sample by extracting and diluting a hot process gas containing condensable components, and uncertainties coupled to dilution are generally overlooked. Some of the artifacts coupled to extraction and dilution may be difficult to interpret and correct.[33] The main concern in this work was to quantify any possible losses in the probe, dilutor, and sampling lines by deposition and diffusion. Alteration of the particle size distribution by agglomeration and condensation is considered less problematic because the objective is to estimate the total mass of alkali per volume.

To estimate deposition losses in the probe, the probe was rinsed before and after each measurement day. The analysis of the probe rinse is given in Table 2 as the deposited mass in the

Table 2. Probe Depositions Per Volume of the Total Pulled Sample Gas through the Probe (mg m^{-3})

day	Na	K	S	Mn	Ni	Cu	Zn	Pb
1	0.07	1.32	0.12	0.01	0.02	0.03	0.03	<0.01
2	0.05	0.95	0.04	0.01	0.01	0.02	0.02	<0.01

probe per the total pulled sample volume (mg m^{-3}). Note that the analysis only provides the mean value during each measurement day and does not reflect the different alkali loadings in the sample gas. Assuming all K deposition as KCl and fully leachable results in a reduced concentration of <1 ppm of KCl of the analyte because of losses in the probe. This indicates that deposition losses in the probe during the specific conditions applied in this study are low. As a result of aerosol dynamics, losses downstream of the probe are considered insignificant,[53] and no correction was performed on the obtained concentration regarding losses in the extraction and dilution downstream of the probe. The correction for dilution was performed by multiplying the dilution ratio (CO_2/$CO_{2\text{-diluted}}$) with the measured CO_2 concentration value. The total dilution ratio (probe tip and porous diluter) was between 1200 and 1600. The aerodynamic quenching at the probe tip in combination with a high dilution appears to be adequate to minimize condensation and deposition losses in the sampling system.

Monitoring of alkali-laden process gas include uncertainties associated with the methodology, sampling, and calibration procedure. Even though some parameters may be kept constant, the true value of the generated alkali concentration in the process gas will always be an unknown parameter. By assessment of random and systematic errors as well as the calibration procedure and extraction, we provide additional knowledge on precision and bias for a SI-based alkali instrument. The favorable agreement between SID and CPFAAS during KCl seeding suggests that the calibration procedure with the SMPS reference provides a reasonable quantification. However, to further reduce uncertainties coupled to the calibration, additional reference methods may be used in future studies, e.g., filter collection or aerosol spectroscopy.

4. CONCLUSION

The applicability and limitations of a SI-based alkali detector have been assessed by internal validation and comparative field measurements with CPFAAS in a simplified technical-scale combustion environment. The presented results demonstrate that a SID is functional to provide quantitative data, as a stand-alone alkali detector, for process gas that contains a known alkali salt composition. The instrument can provide robust continuous measurements over 6−8 h for consecutive days with only a minor instrument drift. For alkali chlorides, the quantified signal is in good agreement with an independent *in situ* laser measurement, using KCl test aerosols and SMPS as a reference. The conformity suggests that extraction, dilution, and conditioning are performed without any significant losses or artifacts. However, for an unknown gas composition, the quantification is hindered by the significant difference in sensitivity for different alkali salts. The investigation of the

internal performance parameters (filament temperature, sample flow, and electric field strength) displayed a low variation in the obtained ion signal, which would generate a satisfactory contribution to the overall measurement uncertainty. Further optimization of filament temperature and electric field strength may allow for discrimination between different alkali salts. As a result of its simplicity, cost-effectiveness, and feature to analyze both gas and particles, the SID is a valuable complementary analytical technique for alkali monitoring of industrial process gas.

■ AUTHOR INFORMATION

Corresponding Author

Dan Gall − *Department of Space, Earth and Environment, Division of Energy Technology, Chalmers University of Technology, SE-412 96 Gothenburg, Sweden;* ● orcid.org/ 0000-0003-3130-8377; Email: dan.gall@chalmers.se

Authors

Jan Viljanen − *Photonics Laboratory, Physics Unit, Tampere University, FI-33101 Tampere, Finland;* ● orcid.org/0000-0002-5992-7199

Ivan Gogolev − *Department of Space, Earth and Environment, Division of Energy Technology, Chalmers University of Technology, SE-412 96 Gothenburg, Sweden*

Thomas Allgurén − *Department of Space, Earth and Environment, Division of Energy Technology, Chalmers University of Technology, SE-412 96 Gothenburg, Sweden;* ● orcid.org/0000-0003-2204-9473

Klas Andersson − *Department of Space, Earth and Environment, Division of Energy Technology, Chalmers University of Technology, SE-412 96 Gothenburg, Sweden;* ● orcid.org/0000-0001-5968-9082

Complete contact information is available at:
https://pubs.acs.org/10.1021/acs.energyfuels.1c03205

Notes

The authors declare no competing financial interest.

■ REFERENCES

(1) International Energy Agency (IEA). *Global Energy Review 2020*; IEA: Paris, France, 2020.

(2) Glarborg, P. Hidden Interactions—Trace Species Governing Combustion and Emissions. *Proc. Combust. Inst.* **2007**, *31* (1), 77−98.

(3) Allgurén, T.; Andersson, K. Chemical Interactions between Potassium, Sulfur, Chlorine, and Carbon Monoxide in Air and Oxy-Fuel Atmospheres. *Energy Fuels* **2020**, *34* (1), 900−906.

(4) Johansson, L. S.; Tullin, C.; Leckner, B.; Sjövall, P. Particle Emissions from Biomass Combustion in Small Combustors. *Biomass Bioenergy* **2003**, *25* (4), 435−446.

(5) Allgurén, T.; Andersson, K. Influence of KCl and SO2 on NO Formation in C3H8 Flames. *Energy Fuels* **2017**, *31* (10), 11413−11423.

(6) McKee, D. W. Mechanisms of the Alkali Metal Catalysed Gasification of Carbon. *Fuel* **1983**, *62* (2), 170−175.

(7) Patwardhan, P. R.; Satrio, J. A.; Brown, R. C.; Shanks, B. H. Influence of Inorganic Salts on the Primary Pyrolysis Products of Cellulose. *Bioresour. Technol.* **2010**, *101* (12), 4646−4655.

(8) Thunman, H.; Seemann, M.; Berdugo Vilches, T.; Maric, J.; Pallares, D.; Ström, H.; Berndes, G.; Knutsson, P.; Larsson, A.; Breitholtz, C.; Santos, O. Advanced Biofuel Production via Gasification—Lessons Learned from 200 Man-Years of Research Activity with Chalmers' Research Gasifier and the GoBiGas Demonstration Plant. *Energy Sci. Eng.* **2018**, 6 (1), 6−34.

(9) Li, K.; Yan, W.; Yu, L.; Huang, X.; Chen, Y.; Zhou, H.; Zheng, S.; Lou, C. Simultaneous Determination of Na Concentration and Temperature during Zhundong Coal Combustion Using the Radiation Spectrum. *Energy Fuels* **2021**, 35 (4), 3348−3359.

(10) Gall, D.; Nejman, C.; Allgurén, T.; Andersson, K.; Pettersson, J. B. C. A New Technique for Real-Time Measurements of Potassium and Sodium Aerosols Based on Field-Reversal Surface Ionization. *Meas. Sci. Technol.* **2021**, 32, 075802.

(11) Morelli, J. J. Thermal Analysis Using Mass Spectrometry: A Review. *J. Anal. Appl. Pyrolysis* **1990**, 18 (1), 1−18.

(12) Heumann, K. G.; Eisenhut, S.; Gallus, S.; Hebeda, E. H.; Nusko, R.; Vengosh, A.; Walczyk, T. Recent Developments in Thermal Ionization Mass Spectrometric Techniques for Isotope Analysis. A Review. *Analyst* **1995**, 120 (5), 1291−1299.

(13) Davidsson, K. O.; Engvall, K.; Hagström, M.; Korsgren, J. G.; Lönn, B.; Pettersson, J. B. C. A Surface Ionization Instrument for On-Line Measurements of Alkali Metal Components in Combustion: Instrument Description and Applications. *Energy Fuels* **2002**, 16 (6), 1369−1377.

(14) Svane, M.; Hagström, M.; Davidsson, K. O.; Boman, J.; Pettersson, J. B. C. Cesium as a Tracer for Alkali Processes in a Circulating Fluidized Bed Reactor. *Energy Fuels* **2006**, 20 (3), 979−985.

(15) Jäglid, U.; Olsson, J. G.; Pettersson, J. B. C. Detection of Sodium and Potassium Salt Particles Using Surface Ionization at Atmospheric Pressure. *J. Aerosol Sci.* **1996**, 27 (6), 967−977.

(16) Andersson, V.; Soleimanisalim, A. H.; Kong, X.; Hildor, F.; Leion, H.; Mattisson, T.; Pettersson, J. B. C. Alkali-Wall Interactions in a Laboratory-Scale Reactor for Chemical Looping Combustion Studies. *Fuel Process. Technol.* **2021**, 217, 106828.

(17) Wellinger, M.; Biollaz, S.; Wochele, J.; Ludwig, C. Sampling and Online Analysis of Alkalis in Thermal Process Gases with a Novel Surface Ionization Detector. *Energy Fuels* **2011**, 25 (9), 4163−4171.

(18) Ji, J.; Cheng, L.; Liu, Y.; Nie, L. Direct Measurement of Gaseous Sodium in Flue Gas for High-Alkali Coal. *Energy Fuels* **2019**, 33 (5), 4169−4176.

(19) Gogolev, I.; Soleimanisalim, A. H.; Linderholm, C.; Lyngfelt, A. Commissioning, Performance Benchmarking, and Investigation of Alkali Emissions in a 10 kW$_{th}$ Solid Fuel Chemical Looping Combustion Pilot. *Fuel* **2021**, 287, 119530.

(20) Andersson, L.; Olsson, J.; Holmlid, L. Surface Ionization at Atmospheric Pressure: Partial Melting of Alkali Salt Particles. *Langmuir* **1986**, 2 (5), 594−599.

(21) Monkhouse, P. B.; Gottwald, U. A.; Davidsson, K. O.; Lönn, B.; Engvall, K.; Pettersson, J. B. C. Phase Discrimination of Alkali Species in PCFB Combustion Flue Gas Using Simultaneous Monitoring by Surface Ionisation and Photofragmentation Fluorescence. *Fuel* **2003**, 82 (4), 365−371.

(22) Gall, D.; Pushp, M.; Larsson, A.; Davidsson, K.; Pettersson, J. B. C. Online Measurements of Alkali Metals during Start-up and Operation of an Industrial-Scale Biomass Gasification Plant. *Energy Fuels* **2018**, 32 (1), 532−541.

(23) Gogolev, I.; Linderholm, C.; Gall, D.; Schmitz, M.; Mattisson, T.; Pettersson, J. B. C.; Lyngfelt, A. Chemical-Looping Combustion in a 100 kW Unit Using a Mixture of Synthetic and Natural Oxygen Carriers—Operational Results and Fate of Biomass Fuel Alkali. *Int. J. Greenhouse Gas Control* **2019**, 88, 371.

(24) Monkhouse, P. On-Line Diagnostic Methods for Metal Species in Industrial Process Gas. *Prog. Energy Combust. Sci.* **2002**, 28 (4), 331−381.

(25) Leffler, T.; Brackmann, C.; Aldén, M.; Li, Z. Laser-Induced Photofragmentation Fluorescence Imaging of Alkali Compounds in Flames. *Appl. Spectrosc.* **2017**, 71 (6), 1289−1299.

(26) Glazer, M. P.; Khan, N. A.; de Jong, W.; Spliethoff, H.; Schürmann, H.; Monkhouse, P. Alkali Metals in Circulating Fluidized Bed Combustion of Biomass and Coal: Measurements and Chemical Equilibrium Analysis. *Energy Fuels* **2005**, 19 (5), 1889−1897.

(27) Qu, Z.; Steinvall, E.; Ghorbani, R.; Schmidt, F. M. Tunable Diode Laser Atomic Absorption Spectroscopy for Detection of Potassium under Optically Thick Conditions. *Anal. Chem.* **2016**, 88 (7), 3754−3760.

(28) Schlosser, E.; Fernholz, T.; Teichert, H.; Ebert, V. In Situ Detection of Potassium Atoms in High-Temperature Coal-Combustion Systems Using near-Infrared-Diode Lasers. *Spectrochim. Acta, Part A* **2002**, 58 (11), 2347−2359.

(29) Forsberg, C.; Broström, M.; Backman, R.; Edvardsson, E.; Badiei, S.; Berg, M.; Kassman, H. Principle, Calibration and Application of the in-Situ Alkali Chloride Monitor (IACM). *Rev. Sci. Instrum.* **2009**, 80 (2), 023104.

(30) Sorvajärvi, T.; Saarela, J.; Toivonen, J. Optical Detection of Potassium Chloride Vapor Using Collinear Photofragmentation and Atomic Absorption Spectroscopy. *Opt. Lett.* **2012**, 37 (19), 4011.

(31) Thorin, E.; Schmidt, F. M. TDLAS-Based Photofragmentation Spectroscopy for Detection of K and KOH in Flames under Optically Thick Conditions. *Opt. Lett.* **2020**, 45 (18), 5230−5233.

(32) *Eurachem Guide: The Fitness for Purpose of Analytical Methods—A Laboratory Guide to Method Validation and Related Topics*, 2nd ed.; Magnusson, B., Örnemark, U., Eds.; Eurachem: Teddington, U.K., 2014.

(33) Jiménez, S.; Ballester, J. A Comparative Study of Different Methods for the Sampling of High Temperature Combustion Aerosols. *Aerosol Sci. Technol.* **2005**, 39 (9), 811−821.

(34) Deuerling, C. F.; Maguhn, J.; Nordsieck, H. O.; Warnecke, R.; Zimmermann, R. Measurement System for Characterization of Gas and Particle Phase of High Temperature Combustion Aerosols. *Aerosol Sci. Technol.* **2010**, 44 (1), 1−9.

(35) Andersson, K.; Johnsson, F. Flame and Radiation Characteristics of Gas-Fired O2/CO2 Combustion. *Fuel* **2007**, 86 (5−6), 656−668.

(36) Ekvall, T.; Andersson, K.; Leffler, T.; Berg, M. K-Cl-S Chemistry in Air and Oxy-Combustion Atmospheres. *Proc. Combust. Inst.* **2017**, 36 (3), 4011−4018.

(37) Bäckström, D.; Gunnarsson, A.; Gall, D.; Pei, X.; Johansson, R.; Andersson, K.; Pathak, R. K.; Pettersson, J. B. C. Measurement of the Size Distribution, Volume Fraction and Optical Properties of Soot in an 80 kW Propane Flame. *Combust. Flame* **2017**, 186, 325−334.

(38) Ionov, N. I. Surface Ionization and Its Applications. *Prog. Surf. Sci.* **1971**, 1, 237.

(39) Sorvajärvi, T.; DeMartini, N.; Rossi, J.; Toivonen, J. In Situ Measurement Technique for Simultaneous Detection of K, KCl, and KOH Vapors Released During Combustion of Solid Biomass Fuel in a Single Particle Reactor. *Appl. Spectrosc.* **2014**, 68 (2), 179−184.

(40) Viljanen, J.; Allgurén, T.; Wang, Y.; Li, X.; Toivonen, J.; Andersson, K.; Wendt, J. O. L. In-Situ Monitoring of Transient Gas Phase K−Cl−S Chemistry in a Pilot-Scale Combustor. *Proc. Combust. Inst.* **2021**, 38, 1823.

(41) Davidovits, P.; Brodhead, D. C. Ultraviolet Absorption Cross Sections for the Alkali Halide Vapors. *J. Chem. Phys.* **1967**, 46 (8), 2968−2973.

(42) Weng, W.; Leffler, T.; Brackmann, C.; Aldén, M.; Li, Z. Spectrally Resolved Ultraviolet (UV) Absorption Cross-Sections of Alkali Hydroxides and Chlorides Measured in Hot Flue Gases. *Appl. Spectrosc.* **2018**, 72 (9), 1388−1395.

(43) Weng, W.; Brackmann, C.; Leffler, T.; Aldén, M.; Li, Z. Ultraviolet Absorption Cross Sections of KOH and KCl for Nonintrusive Species-Specific Quantitative Detection in Hot Flue Gases. *Anal. Chem.* **2019**, 91 (7), 4719−4726.

(44) Sorvajärvi, T.; Toivonen, J. Principles and Calibration of Collinear Photofragmentation and Atomic Absorption Spectroscopy. *Appl. Phys. B: Lasers Opt.* **2014**, 115 (4), 533−539.

(45) Bäckström, D.; Gall, D.; Pushp, M.; Johansson, R.; Andersson, K.; Pettersson, J. B. C. Particle Composition and Size Distribution in

Coal Flames—The Influence on Radiative Heat Transfer. *Exp. Therm. Fluid Sci.* **2015**, *64*, 70−80.

(46) Jensen, J. R.; Nielsen, L. B.; Schultz-Møller, C.; Wedel, S.; Livbjerg, H. The Nucleation of Aerosols in Flue Gases with a High Content of Alkali—A Laboratory Study. *Aerosol Sci. Technol.* **2000**, *33* (6), 490−509.

(47) Lyyränen, J.; Jokiniemi, J.; Kauppinen, E. I.; Backman, U.; Vesala, H. Comparison of Different Dilution Methods for Measuring Diesel Particle Emissions. *Aerosol Sci. Technol.* **2004**, *38* (1), 12−23.

(48) Dresser, M. J. The Saha-Langmuir Equation and Its Application. *J. Appl. Phys.* **1968**, *39* (1), 338−339.

(49) Gall, D.; Pushp, M.; Davidsson, K. O.; Pettersson, J. B. C. Online Measurements of Alkali and Heavy Tar Components in Biomass Gasification. *Energy Fuels* **2017**, *31* (8), 8152−8161.

(50) Lüönd, F.; Schlatter, J. Improved Monodispersity of Size Selected Aerosol Particles with a New Charging and Selection Scheme for Tandem DMA Setup. *J. Aerosol Sci.* **2013**, *62*, 40−55.

(51) Kowalski, T.; Ludwig, C.; Wokaun, A. Qualitative Evaluation of Alkali Release during the Pyrolysis of Biomass. *Energy Fuels* **2007**, *21* (5), 3017−3022.

(52) Datz, S.; Taylor, E. H. Ionization on Platinum and Tungsten Surfaces. I. The Alkali Metals. *J. Chem. Phys.* **1956**, *25* (3), 389−394.

(53) Hinds, W. *Aerosol Technology*, 2nd ed.; John Wiley & Sons: Hoboken, NJ, 1998.

(54) Biskos, G.; Vons, V.; Yurteri, C. U.; Schmidt-Ott, A. Generation and Sizing of Particles for Aerosol-Based Nanotechnology. *KONA Powder Part. J.* **2008**, *26*, 13−35.

(55) Park, K.; Kim, J.-S.; Miller, A. L. A Study on Effects of Size and Structure on Hygroscopicity of Nanoparticles Using a Tandem Differential Mobility Analyzer and TEM. *J. Nanopart. Res.* **2009**, *11* (1), 175−183.